RESEARCH
SIGNPOST

Focusing light with fractal zone plates

Juan A. Monsoriu[1], Walter D. Furlan[2] and Genaro Saavedra[2]
[1]Departamento de Física Aplicada, Universidad Politécnica de Valencia
E-46022 Valencia, Spain; [2]Departamento de Óptica, Universitat de València
E-46100 Burjassot, Spain

Abstract

A detailed description of the design procedure of fractal zone plates (FZPs), i.e., zone plates with fractal structure, is given. The focusing properties of these elements are studied analytically and compared with conventional Fresnel zone plates. Some distinctive aspects of the new kind of zone plates are outlined. It is shown that the axial irradiance exhibited by the FZP has self-similarity properties that can be correlated to those of the diffracting aperture. In addition, the impact on the axial irradiance produced by the lacunarity of a general FZP is investigated. Several numerical examples that illustrate these features are presented.

Correspondence/Reprint request: Dr. Walter D. Furlan, Departamento de Óptica, Universitat de València C/Dr. Moliner, 50. E-46100 Burjassot, Spain. E-mail: walter.furlan@uv.es

1. Introduction

A renewed interest in zone plates [1] has been experienced during the last years because they are becoming key elements in obtaining images in several scientific and technological areas such as THz tomography and soft X-ray microscopy [2-6]. With this motivation, we have recently proposed fractal zone plates (FZPs) as new promising 2D photonic structures [7-10]. Under certain circumstances, a FZP can be thought as a conventional zone plate with certain missing zones. The resulting structure is characterized by its fractal profile along the square of the radial coordinate.

In this text we show that the axial irradiance provided by a FZP when illuminated with a parallel wavefront presents multiple foci, the main lobe of which coincide with those of the associated conventional zone plate. The internal structure of each focus exhibits a characteristic fractal structure, reproducing the self-similarity of the originating FZP. In addition, we analyze the axial response of FZPs to a specific design parameter, frequently used as a measure of the "texture" of fractal structures: the lacunarity. Some practical considerations about the design of this general type of FZPs are investigated, taking into account the physical limits imposed by the different construction parameters. The axial irradiance provided by FZPs with variable lacunarity is numerically evaluated, and compared with the response of regular FZPs. Finally, since a simple theoretical relation is found between the transmittance of the FZP and their axial response, synthesis of axial irradiances with fractal profile can be easily achieved.

2. Theory

Let us start by considering the irradiance at a given point on the optical axis, provided by a rotationally invariant pupil function described by $p(r)$, illuminated by a monochromatic plane wave. Within the Fresnel approximation, this magnitude is given as a function of the axial distance from the pupil plane z, as

$$I(R) \doteq \left(\frac{2\pi}{\lambda z}\right)^2 \left| \int_0^a p(r_o) \exp\left(-\mathrm{i}\frac{\pi}{\lambda z} r_o^2\right) r_o \, \mathrm{d}r_o \right|^2 \tag{1}$$

In Eq. (1), a is the maximum extent of the pupil function, and λ is the wavelength of the light. For our purposes it is convenient to express the pupil transmittance as function of a new variable defined as

$$\varsigma = \left(\frac{r_o}{a}\right)^2 - 0.5, \tag{2}$$

in such a way that $q(\varsigma)=p(r_o)$. By using the dimensionless axial coordinate $u = a^2/2\lambda z$, the irradiance along the optical axis can be now expressed as

$$I_o(u) = 4\pi^2 u^2 \left| \int_{-0.5}^{+0.5} q(\varsigma) \exp(-i2\pi u\varsigma)\, d\varsigma \right|^2 .$$

(3)

From this result it is straightforward to note that the behaviour of $I_o(u)$ is basically governed by the square modulus of the Fourier transform of $q(\varsigma)$.

Let us now consider a pupil function $q(\varsigma)$ that holds a fractal structure. Thus, from well-known properties of fractals and their Fourier transforms [11], it is direct to conclude that such element will provide an irradiance along the optical axis with a fractal profile. We called this kind of pupils fractal zone plates (FZPs) because, as we will see next, they can be constructed from conventional Fresnel zone plates in some cases. Although in the construction of a FZP any fractal 1-D structure can be used, we will focus our attention on binary Cantor sets.

As it is well known, a Fresnel zone plate consists of alternately transparent and opaque zones whose radii are proportional to the square root of the natural numbers. By using Eq. (2), it is easy to obtain that the function $q(\varsigma)$ for these pupils is a Ronchi-type periodic binary function with period p (see Fig. 1a), that can be written as

$$q(\varsigma) = q_{ZP}(\varsigma, p) = \mathrm{rect}(\varsigma)\, \mathrm{rect}\left(\frac{\mathrm{mod}(\varsigma + \frac{p-1}{2}, p)}{p} \right),$$

(4)

where the function $\mathrm{mod}(x, y)$ gives the remainder on division of x by y.
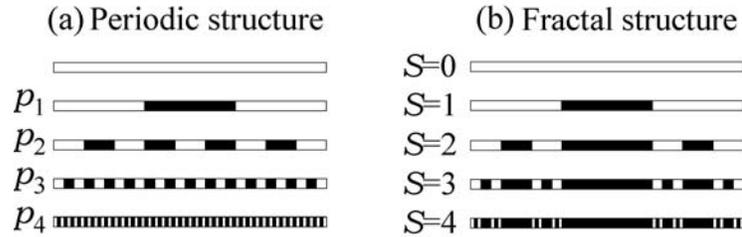
Figure 1. Schemes for the generation of the binary function $q(\varsigma)$ for: (a) Fresnel zone plate with different periods $p_S=p(N,S)$, for $N=2$ and different values of S; (b) its associated FZP. In this representation clear and dark segments correspond to the values 1 and 0 of the generating binary function, respectively.

In a similar way, FZPs are constructed by replacing the above 1-D periodic function by a 1-D binary function with fractal profile. Consider, for example, the particular case of a regular Cantor fractal whose construction procedure is shown in Fig. 1b). In the first stage ($S=1$), the initial segment is divided into an odd number of segments $2N-1$ and the segments in the even positions are removed (in the figure a triadic Cantor set was considered, thus $2N-1=3$). For the remaining N segments at the first stage, this "slicing and removing" process is repeated in the second stage and so on. In mathematical terms, the FZP transmittance function, developed up to a certain "growing" stage S, can be expressed as the product of the periodic functions $q(\varsigma)$ in Eq. (4) as

$$q(\varsigma) = q_{FZP}(\varsigma, N, S) = \prod_{i=0}^{S} q_{ZP}\left(\varsigma, \frac{2}{(2N-1)^i}\right).$$ (5)

It is instructive to note that the FZP in Eq.(5) can be understood as an associated Fresnel zone plate $q_{ZP}[\varsigma, p(N,S)]$, with period

$$p(N,S) = \frac{2}{(2N-1)^S},$$ (6)

but with some missing clear zones (compare Fig. 1a with Fig. 1b). Figure 2 shows a FZP generated from a triadic Cantor set, up to $S=3$, and the corresponding Fresnel zone plate with period $p(2,3)$.
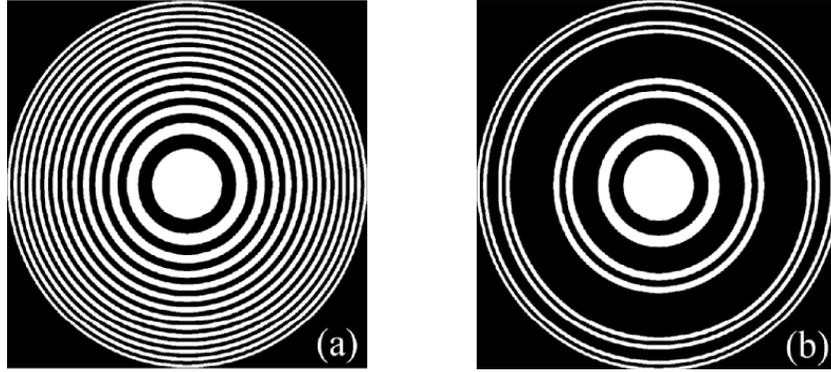
Figure 2. Fresnel zone plate (a) and the associated FZP (b) generated from the 1-D functions in Fig. 1 for $S=3$. The generating process consists in rotating the respective whole structure around one extreme after the change of variables in Eq. (2).

To compare the axial behavior of a FZP with its associated Fresnel zone plate, we will obtain analytically the axial irradiance distributions (I_0^{FZP} and I_0^{ZP}, respectively) in both cases. For the first case, from the recursive building procedure of the FZP and proper use of the convolution theorem for the Fourier transform in Eq. (3) it is easy to obtain that

$$I_0^{FZP}(u,N,S) = 4\sin^2\left(\frac{\pi u}{(2N-1)^S}\right)\prod_{i=1}^{S}\frac{\sin^2\left[\dfrac{2\pi N u}{(2N-1)^i}\right]}{\sin^2\left[\dfrac{2\pi u}{(2N-1)^i}\right]}. \tag{7}$$

For the associated Fresnel zone plate, Eq. (3) leads to the well-know result [12]

$$I_0^{ZP}(u,N,S) = \frac{\sin^2\left[\dfrac{2\pi M u}{(2N-1)^S}\right]}{\cos^2\left[\dfrac{\pi u}{(2N-1)^S}\right]}. \tag{8}$$

In Eq. (8) M is the number of transparent Fresnel zones and is given by $\lceil (2N\text{-}1)^S/2 \rceil$, where $\lceil x \rceil$, called the ceiling of x, denotes the smallest integer greater than, or equal to, x.

The axial irradiance of the FZP computed for different stages of growth S and for $N=2$ is shown in Fig. 3. The irradiance of the associated Fresnel zone plate is shown in the same figure for comparison. Note that the scale for the axial coordinate in each step is a demagnified version of the one in the previous step by a factor $2N-1 = 3$. It can be seen that the axial positions of the central lobes of the foci coincide with those of the associated Fresnel zone. It is clear that, while the internal structure of each focus in the Fresnel zone plate vanish progressively, the axial response for the FZP exhibits its characteristic fractal profile. In fact, the four patterns in the upper part of Fig. (3) are self-similar. We called this scaling property along the optical axis, that holds for any N, the *axial scale property*. This means that the axial irradiance reproduce the self-similarity of the FZP.

In order to see the fractal behavior of the internal structure of the FZP foci, a more convenient representation of the axial irradiance can be achieved by noting that the irradiances in Eq. (7) and Eq. (8) are periodic functions of u, with period $u_p=(2N-1)^S$. Thus, through the change of variables $u_N=u/u_p$, we obtain

$$I_0^{FZP}(u_N, N, S) = 4\sin^2(\pi u_N)\prod_{i=1}^{s}\frac{\sin^2\left[2\pi N(2N-1)^{S-i}u_N\right]}{\sin^2\left[2\pi(2N-1)^{S-i}u_N\right]} \ . \tag{9}$$

This last result for the FZP is shown in Fig. 4. It can be seen that the axial irradiance for a given stage S is a modulated version of that associated with the previous stage. In our case, as S increases, an increasing number of zeros and maxima are encountered which are scale invariant over dilations of factor $2N-1 = 3$, as corresponds to a self-similar structure. As in the case of a Fresnel zone plate, the axial irradiance behavior of the FZP can easily be interpreted as the interference between the successive rings over the pupil.

For both the FZP and the ZP the main focus occurs at normalized value $u_N = 0.5$ that correspond to a focal length

$$f(N,S) = \frac{a^2}{\lambda(2N-1)^s} \ . \tag{10}$$

Note that although Figs. 3 and 4 seem to show that the axial irradiance is symmetric around each focus, it doesn't stands if we represent this function versus the true axial distance z. This fact is illustrated in Fig. 5.
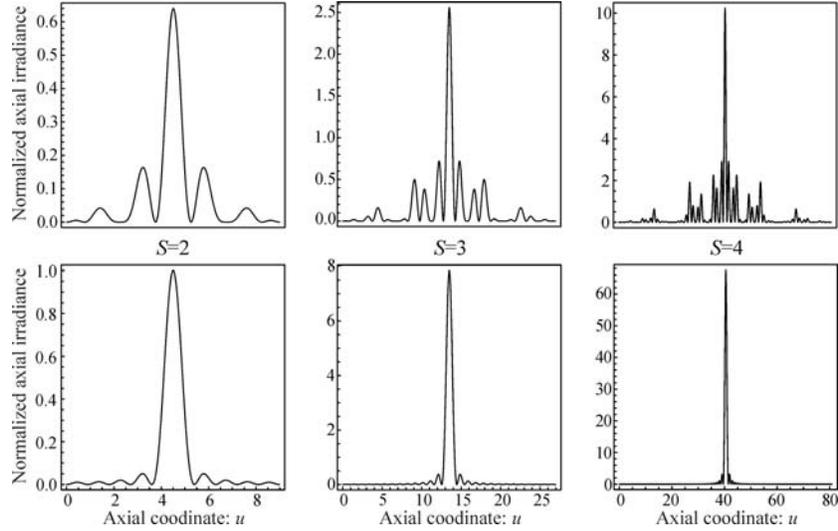
Figure 3. Normalized irradiance vs. the axial coordinate u obtained for a FZP at four stages of growth (upper part) and for its associated Fresnel zone plate (lower part). In all cases $N=2$.
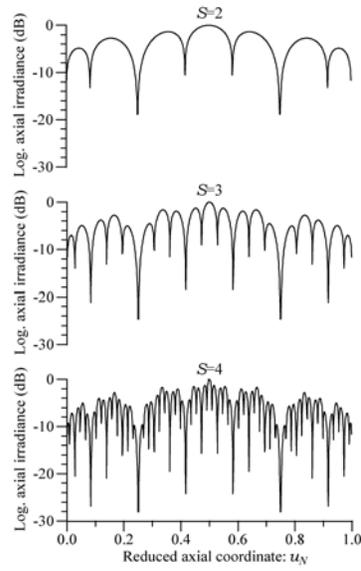
Figure 4. Log plot of axial irradiances vs. the reduced axial coordinate u_N obtained from the plots in the upper part of Fig. 3.
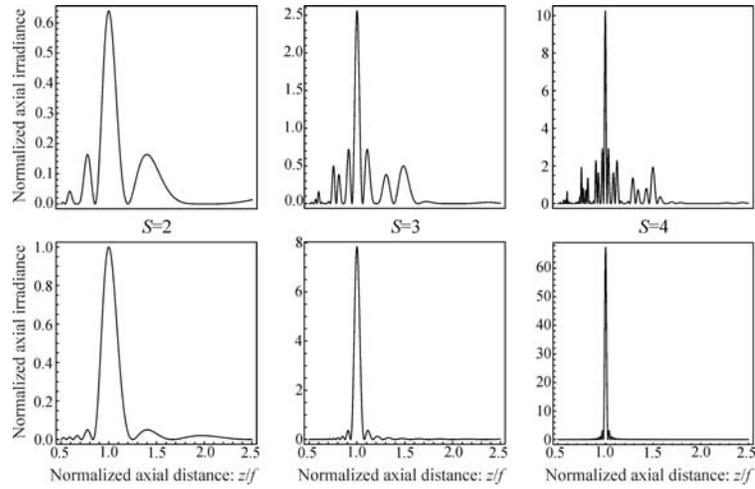
Figure 5. Normalized irradiance vs. the axial distance z (from the pupil plane) obtained for a FZP at four stages of growth (upper part) and for its associated Fresnel zone plate (lower part). In all cases $N=2$. The axial distance is normalized to the focal length $f=f(N,S)$ given by Eq.(10). For simplicity we display a region up to $z=2.5f$.

3. Lacunarity in fractal zone plates

In the previous section the FZP considered were constructed from regular fractal structures in the sense that (as can be seen in Fig. 1b) the clear and dark regions have the same size. A more general FZP can be defined when another design parameter is taken into account: the lacunarity. The construction of a typical *polyadic* Cantor fractal set with a specific lacunarity is shown in Fig. 6. The first step in the construction procedure consists in defining a straight-line segment of unit length called *initiator* (stage $S=0$). Next, at stage $S=1$, the *generator* of the set is constructed by N ($N=4$ in the figure) non-overlapping copies of the initiator each one with a scale $\gamma<1$. At the following stages of construction of the set ($S=2,3,...$), the generation process is repeated over and over again for each segment in the previous stage. To characterize the resulting Cantor set, as well as many other fractal structures, one of the most frequently-used descriptors is the *fractal dimension*, defined as

$$D = -\frac{\ln(N)}{\ln(\gamma)} .\tag{11}$$

However, this parameter does not uniquely define the fractal. In fact, for the most general case, it is necessary to introduce another parameter to specify the distribution of the N copies into the unit length segment. This parameter specifies the lacunarity (or "gapinness") of the resulting structure. In other words, structures with different lacunarity can have the same fractal dimension. As in previous papers dealing with Cantor fractals in Optics [13,14], the width of outermost gap in the first stage, ε (see Fig. 6) was used here for this purpose. However, the construction parameters of a FZP are not independent, and so they must satisfy the following constraints. On the one hand, the maximum value of the scale, γ_{max}, depends on the value of N, i.e., $0 \leq \gamma_{max} \leq N^{-1}$. On the otherhand, for each value of N and γ, there are two extreme

Figure 6. Schemes for the generation of the FZP binary function $q(\varsigma)$ for $N=4$ up to $S=2$. γ is the scale factor and ε is the parameter that characterizes the lacunarity.

values for ε. For the first, $\varepsilon=0$, the result is the highest lacunar fractal, having the central gap very large while the outer ones become null. The other extreme value of ε is

$$\varepsilon_{max} = \frac{1-N\gamma}{N-2}.$$ (12)

In this case, a lower lacunar structure than in the previous case is obtained, since the central gap is missed. Between *zero* and ε_{max} there exists a particular value of ε that gives the lowest lacunar (or *regular*) fractal. This value of ε, obtained by imposing bars and gaps to have the same size at the initiatior stage (as done in Ref. [7]), is given by

$$\varepsilon_R = \frac{1-N\gamma}{N-1}.$$ (13)

The influence of these construction parameters is shown in Fig. 7. FZPs are generated by mapping the Cantor bars (like the one in the middle row of Fig. 6, i.e., $N=4$ and $S=1$) by use of Eq. (2), and rotating the re-scaled bars around one of the extremes. FZPs for different values of γ and ε are presented.

Summarizing, the number of stages, the lacunarity, the fractal dimension, and the scale, are the independent variables in the construction of a FZP. The influence of them on the axial irradiance given by Eq. 3 will be presented bellow.

Since for the regular case the axial irradiance is a periodic funtion of the coordinate u with period $u_p=1/\gamma^S$, the most graphical way to observe the axial fractal behavior of the irradiance is by defining the reduced axial coordinate as $u/u_p=\gamma^S u$. Figure 8 (top) shows the FZP constructed with $\gamma=1/7$ and the same values of ε as in Fig. 7, but for $S=2$. The normalized axial irradiances given by these pupils are represented with solid line in Fig. 8 (bottom). Also, we have represented in dashed line the axial irradiances given by the corresponding FZP for $S=1$. From Fig. 8 it is obvious that the optical irradiance produced by the FZPs is highly influenced by the lacunarity. Besides, for the regular FZP (Fig. 8 middle), the self-similarity between these patterns can be clearly seen: the solid line pattern is a magnified version of the dashed one, and this one is an envelope of the former.

Although from this figure it seems that the self-similarity observed for the regular FZP ($\varepsilon=\varepsilon_R$) is not supported by other values of ε, this effect is an artifact due to the scale and range used in this figure. Another interesting result which is masked in Fig. 8 by the use of the normalized axial coordinate is that there are certain axial positions with zero axial irradiance for all values of ε. All these effects can be better seen in Fig. 9.
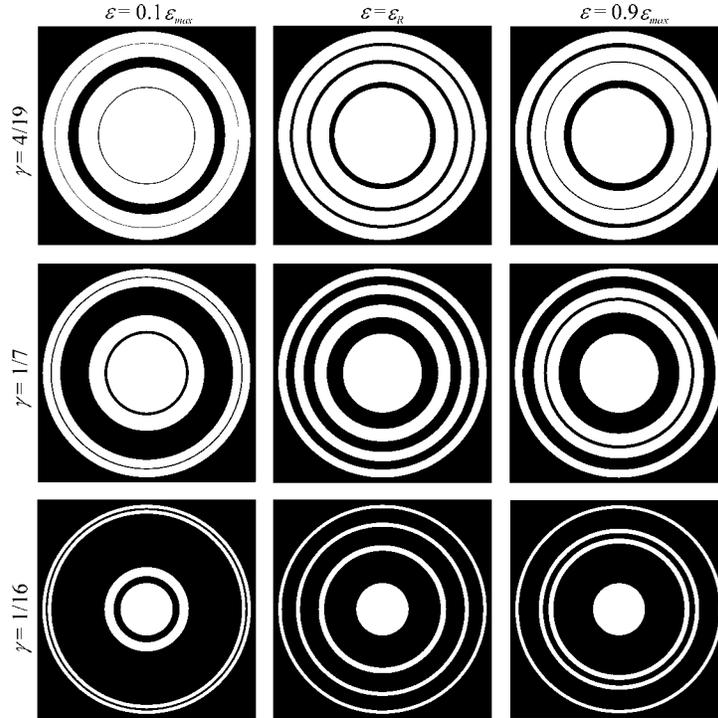
Figure 7. FZPs generated with three different values of γ and three different lacunarity ε. Note that ε_{max} is different in each case being 3/38 (top); 3/14 (center line) ; and 3/8 (bottom).

In this figure the axial coordinate is extended to cover several periods of the regular case. In this figure normalized axial irradiances (as a function of u) are represented as gray levels for six families of FZPs: three with the same γ as in Fig. 7 corresponding to S=1 (left) and other three with the same parameters but for S=2 (right). These irradiances were computed for the whole range of ε and then stacked sequentially to obtain these 2D displays (usually called *twist plots* [13]). The first common aspect to be noted in all pictures is that there are vertical dark bands corresponding to axial nulls whose positions remain invariant with the lacunarity. These nulls are obtained at values $u= i/\gamma^{S}$ (for i=1, 2, ...), and are caused by the destructive axial interference between all points inside each individual ring with the same scale factor γ. In a similar way, the other nulls in this figure can be understood as multiple cross-interferences between different rings of the FZP. At this point it is interesting to note that the re-scaled data in the stage S=1 form an envelope for the data at
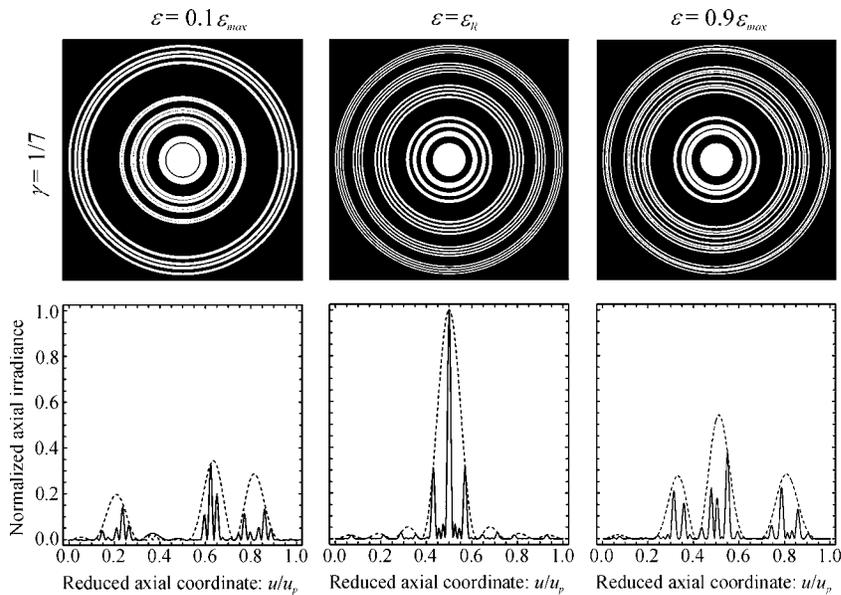
Figure 8. Top: FZPs generated with $\gamma=1/7$, the same values of ε as in Fig. 7, and $S=2$. Bottom: Normalized axial irradiances obtained with theses pupils for $S=2$ (solid lines) and for $S=1$ (dashed lines).

the $S=2$ one and both structures are self-similar for any value of ε. A similar behavior for other Cantor-related structures was previously reported [13,14].

To analyze how the lacunarity affects the axial irradiance, we can use a generalization of the correlation degree defined by Sakurada *et al.* [15] for measuring the self-similarity. In our case the axial irradiances for a variable lacunarity were correlated with the same function computed for $\varepsilon=\varepsilon_R$, since for this particular value the self-similarity exhibited by the axial irradiance reproduces the self-similarity of the FZP. Note that this case also corresponds to the lowest lacunar FZP. Thus, we use the correlation coefficient given by

$$C(\varepsilon)=\frac{\int_0^\infty I_{\varepsilon_R}(u)\cdot I_\varepsilon(u)\,du}{\sqrt{\int_0^\infty I_{\varepsilon_R}^2(u)\,du\;\int_0^\infty I_\varepsilon^2(u)\,du}}\,. \tag{14}$$

From its definition, the function $C(\varepsilon)$ is expected to be a continuous function, having an absolute maximum value of unity at $\varepsilon=\varepsilon_R$. Since the
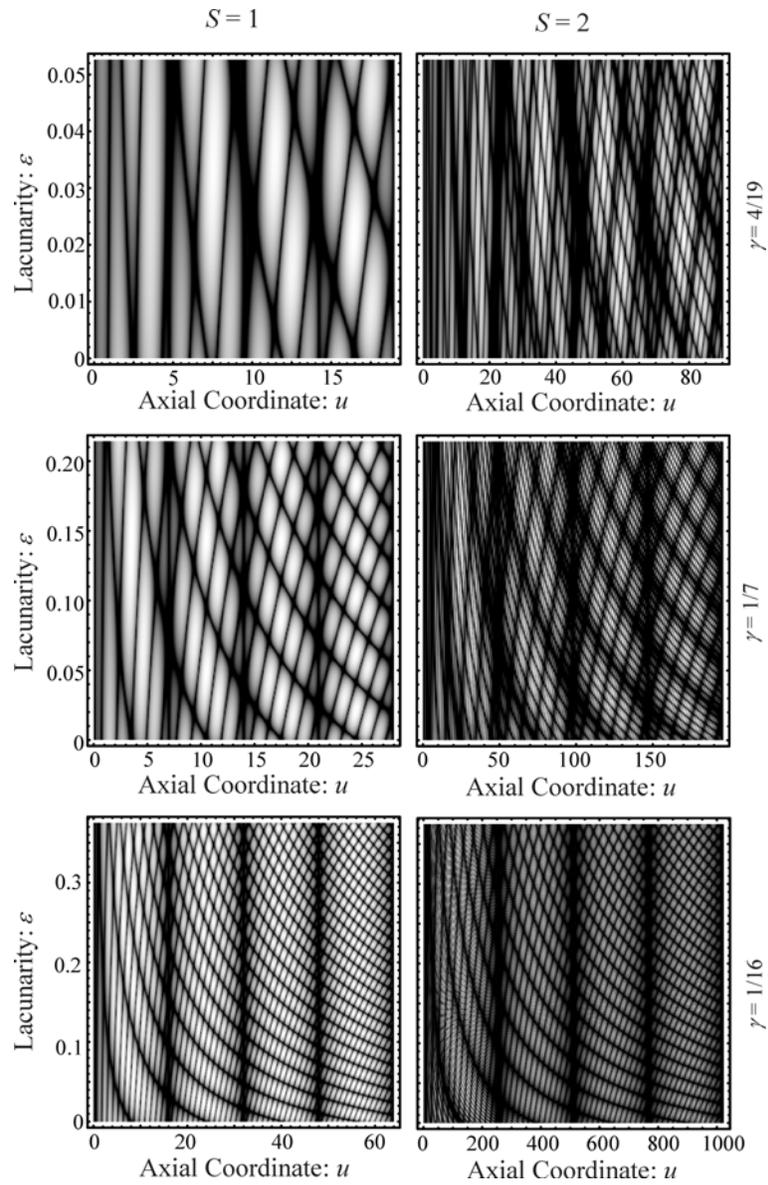
Figure 9. Gray–scale representation of the axial irradiance (in dB) plotted as a function of the normalized axial coordinate and the lacunarity (*twist plots*) with the same values of γ as in Fig. 7. Left and right correspond to $S=1$ and $S=2$, respectively.

infinite limits in the integrations in Eq. (14) would pose difficulties to the accurate numerical evaluation of $C(\varepsilon)$, a more convenient expression can be obtained by using Eq. (3) and the Rayleigh's theorem. In this way, $C(\varepsilon)$ can be expressed as

$$C(\varepsilon) = \frac{\int_{-1}^{1}\left[q_{\varepsilon_R}(\varsigma) \otimes q_{\varepsilon_R}(\varsigma)\right]\cdot\left[q_{\varepsilon}(\varsigma) \otimes q_{\varepsilon}(\varsigma)\right]d\varsigma}{\sqrt{\int_{-1}^{1}\left[q_{\varepsilon_R}(\varsigma) \otimes q_{\varepsilon_R}(\varsigma)\right]^2 d\varsigma \ \int_{-1}^{1}\left[q_{\varepsilon}(\varsigma) \otimes q_{\varepsilon}(\varsigma)\right]^2 d\varsigma}}. \tag{15}$$

where $\otimes$ represents the convolution operation. With this definition the integrals in Eq. (15) are compact supported and the degree of similarity between axial irradiances can be more precisely numerically evaluated. The function $C(\varepsilon)$ was computed for different values of S. The result is shown in Fig. 10. Compared with the result obtained for $S=1$ (dashed line) the correlation coefficient for $S=2$ (solid lined) present a higher number of maxima and minima and seems to be a modulated version of the previous stage. Thus, the function $C(\varepsilon)$ has fractal properties itself to a certain extent, though limited for the range of ε available for each value of γ. This last result is another property of FZPs.
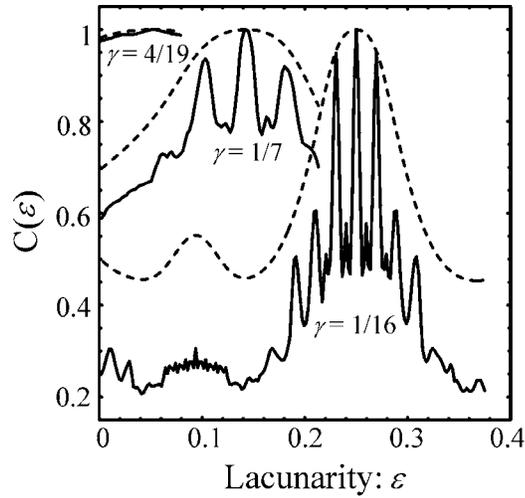
Figure 10. $C(\varepsilon)$ for the FZPs for $S=2$ (solid line) and $S=1$ (dashed line) with the same values of γ as in Fig. 7.

4. Conclusions

Regular FZPs and FZPs with variable lacunarity have been extensively analyzed. The construction restrictions and the interrelations between the different parameters has been investigated. We have shown that the irradiance along the optical axis produced by these pupils shows a characteristic fractal profile. The lacunarity has a dramatic effect on the axial irradiance provided by different FZPs with the same fractal dimension; however, certain aspects of the self-similarity are preserved.

The present study brings new lights on the powerful potential applications of FZPs, especially in scientific and technological areas where conventional zone plates have been successfully applied. Particularly, recent proposals of optical tweezers use phase filters to facilitate the trapping of particles in three-dimensional structures [16]; spatial light modulators can be employed to display tunable FZPs producing focal spots that could be useful for these purposes. On the other hand, the non-uniform distribution of FZPs focal points along the optical axis could be exploited in ophthalmology for the design of multifocal contact or intra-ocular lenses for the correction of presbyopia. In this case, a mechanism to control the diffraction efficiency of the FZP should be first developed. Besides of the influence of optical aberrations, and polychromatic illumination on different geometries of FZPs, currently we are investigating non-binary FZPs and their properties.

5. Acknowledgments

6. References

1. J. Ojeda-Castañeda and C. Gómez-Reino, Eds., *Selected papers on zone plates* (SPIE Optical Engineering Press, Washington, 1996).
2. *S*. Wang and X. Zhang, *Terahertz tomographic imaging with a Fresnel lens*, Opt. Photon. News **13**, 59 (2002).
3. Y Wang, W. Yun, and C. Jacobsen, *Achromatic Fresnel optics for wideband extreme-ultraviolet and X-ray imaging*, Nature **424**, 50-53 (2003).
4. L. Kipp, M. Skibowski, R. L. Johnson, R. Berndt, R. Adelung, S. Harm, and R. Seemann, *Sharper images by focusing soft x-rays with photon sieves*, Nature **414**, 184-188 (2001).
5. Q. Cao and J. Jahns, *Modified Fresnel zone plates that produce sharp Gaussian focal spots*, J. Opt. Soc. Am. A **20**, 1576-1581 (2003).

6. Q. Cao and J. Jahns, *Comprehensive focusing analysis of various Fresnel zone plates*, J. Opt. Soc. Am. A **21**, 561-571 (2004).

7. G. Saavedra, W.D. Furlan, and J.A. Monsoriu, *Fractal zone plates*, Opt. Lett. **28**, 971-973 (2003).

8. W.D. Furlan, G. Saavedra, and J.A. Monsoriu, *Fractal zone plates produce axial irradiance with fractal profile*, Opt.& Photon. News **14**(12), 31 (2003).

9. J.A. Monsoriu, G. Saavedra, and W.D. Furlan, *Fractal zone plates with variable lacunarity*, Opt. Express **12**, 4227-4234 (2004).

10. J.A. Davis, L. Ramirez, J.A. Rodrigo Martín-Romo, T. Alieva, and M.L. Calvo, *Focusing properties of fractal zone plates: experimental implementation with a liquid-crystal display*, Opt. Lett. **29**, 1321-1323 (2004).

11. J. Uozumi and T. Asakura, *Fractal Optics, Current Trends in Optics Ch.* **6**, J.C. Dainty Ed., Academic Press, London (1994).

12. A. Boivin, *On the theory of diffraction by concentric arrays of ring-shaped apertures*, J. Opt. Soc. Am **42**, 60-64 (1952).

13. A.D. Jaggard and D.L. Jaggard, *Cantor ring diffractals, Opt. Commun.* **158**, 141–148 (1998).

14. L. Zunino and M. Garavaglia, *Fraunhofer diffraction by Cantor fractals with variable lacunarity*, J. Mod. Opt. **50**, 717-727 (2003).

15. Y. Sakurada, J. Uozumi, and T Asakura, *Fresnel diffraction by 1-D regular fractals*, Pure Appl. Opt. **1**, 29–40 (1992).

16. H. Melville and G. F. Milne, *Optical trapping of three-dimensional structures using dynamic holograms*, Opt. Express **11**, 3562-3567 (2003).